Highly crystalline silicon carbide of controlled mesoporosity

B. Gouze, K.B. Cervantes-Diaz, T. Nardin, O. Diat, J. Cambedouzou

Version of Record: https://www.sciencedirect.com/science/article/pii/S0254058420305794
Manuscript_4c7ae1817286644d88e624feb1e1d6e8

Highly crystalline silicon carbide of controlled mesoporosity

B. Gouze[1], K. Cervantes[2], T. Nardin[1, †] O. Diat[1] and J. Cambedouzou[1,2,*]

[1] Institut de Chimie Séparative de Marcoule, CEA, CNRS, ENSCM, Univ Montpellier, Marcoule, France
[2] Institut Européen des Membranes CNRS, ENSCM, Univ Montpellier, Montpellier, France
[†] Present address: IFP Energies nouvelles, Solaize, France

*Corresponding author: julien.cambedouzou@enscm.fr

Keywords: Silicon carbide, mesoporous ceramics, soft-templating, block copolymers

Abstract

The control of porosity in silicon carbide (SiC) at the mesoporous scale is a major concern for a range of separation applications. It was recently reported that mesoporous amorphous SiC could be synthesized by templating polycarbosilane precursors around polymeric templates, and after pyrolysis at 1000°C under inert atmosphere. In this publication, we report the synthesis of highly crystalline mesoporous β-SiC based on the same approach, but involving much higher temperature pyrolyses (up to 1900°C). The structure evolution with regards to the pyrolysis temperature is carefully studied by means of various analytical tools. Finally, the influence of different synthesis parameters on the control of the mesoporous structure is also discussed. It is shown for the first time that pure mesoporous β-SiC with 10 nm pore diameter and a specific surface area larger than 50 m^2/g can be obtained with a very high degree of crystallinity.

1. Introduction

The exceptional mechanical and thermal properties of silicon carbide (SiC) make this material highly desirable for a range of applications such as gas filtration [1], photocatalyst for hydrogen production [2,3] and removal of organic dyes [4,5]. Moreover, the hydrophobic character of its surface [6] opens new fascinating opportunities as a porous material for water filtration and separation applications. Controlling the porosity in such cohesive materials is however challenging. Porous SiC membranes obtained by recrystallization techniques [7] are commercially available (e.g. at St Gobain, CoMeTas, CeraMem), but their pore diameter is too large to ensure competitive performances for low-ultrafiltration and nanofiltration. Templating approaches appear as promising processes in order to control SiC porosity with typical pore diameters lower than 50 nm. It has been shown that mesopororous silica can be considered as hard templates resulting in rod-like SiC, showing high specific surface area [8,9]. Likewise, polycarbosilane (PCS) infiltration method with silica nanofoam as template led to synthesis of SiC nanofoams with a controlled porosity and pore size ranging between

10 and 100 nm [10]. However, template elimination requires the use of harsh conditions, often involving hydrofluoric acid. It is therefore preferable to use more durable processes, where the template is directly built in the liquid media constituted by the SiC precursors and can sometimes be further recycled. This so-called "soft-templating" approach has thus been used to produce nanoporous SiC, involving molecular or polymeric templating agents, which can be e.g. semifluorinated alkanes [11,12] in the first case, or block copolymers [13–20] in the second case. Concerning approaches involving block-copolymers, it has been reported the synthesis of nanostructured SiC with a grain size of approximately 30 nm by self-assembly of polyvinylsilazane-block- polystyrene (PVSZ-b-PS) block copolymers and SiC precursor followed by pyrolysis at 800 °C to form nanoporous SiC [16]. Furthermore, resizing the two blocks of the copolymer leads to change the pore size of mesoporous SiC [17], highlighting the potential of this approach in terms of pore size control. We have proposed in the meantime a slightly different approach where allylhydridopolycarbosilane (AHPCS) is used as SiC precursor and a polystyrene-*block*-polybutadiene-*block*-polystyrene denoted SBS is used as a porogen agent [18]. SBS is able to self-assemble both as pure or diluted in a solvent due to a nano-phase separation between the polystyrene (PS) blocks and the polybutadiene (PB) blocks [19]. As AHPCS has no preferential affinity for the PS or the PB phase, it was selectively grafted by catalyzed hydrosilation to the PB blocks of the SBS. PS aggregates acted as templating agents before being removed by a pyrolysis step at a temperature higher than 500°C, thus releasing porosity in the material. After a 1000°C under Ar atmosphere, a SiC material with an amorphous structure was recovered, showing a specific surface area higher than 400 m^2/g and an averaged pore size of about 4 nm.

Recently, mesoporous nanostructured SiC has been obtained by soft-templating AHPCS with triblock copolymer poly(methylmethacrylate)-bpoly(n-butylacrylate)-b-poly(methylmethacrylate) (denoted as PMBM) without an annealing step to reach materials self-assembly. Removing of the PMBM template and conversion of AHPCS into the SiC structure (worm-like mesopores surrounded by an amorphous interconnected ceramic strut structure) occurred after pyrolysis at 800°C with a conversion yield of approximately 80 wt % [20].
In all these strategies, amorphous SiC materials, still containing amounts of hydrogen and/or nitrogen (depending on the precursor used) is produced regarding the rather low pyrolysis temperatures (800°C to 1000°C). A major subsisting interrogation is the ability of such soft-templating approaches to deliver a highly crystalline SiC material conserving a high specific surface area, i.e. are these self-assembled structures able to endure a thermal treatment at 1900°C for a few hours without losing their porosity. The production of SiC combining a very high porosity and a perfectly defined crystalline structure is yet highly desirable for applications requiring high mechanical resistance and well-defined bandgap, such as water treatment by photodegradation.

Based on the promising results obtained in [18], we studied further in detail this elaboration strategy by bringing some specific modifications to the protocol described in this reference. Therefore, we considered in more detail the effect of the crosslinking step using $Cp_2Ti(OPh)_2$

as a catalyst before pyrolysis of the mixture. We also gave a peculiar attention to the effect of the weight ratio between the SBS structuring agent and the AHPCS precursor. Last, we studied in detail the effect of the pyrolysis temperature by performing a multi-method analysis of the material after pyrolyses made at 1000°C, 1300°C, and 1900°C. These different temperatures are considered as key temperatures related to different chemical compositions and crystallographic structures with regard to AHPCS evolution [21]. A peculiar attention was given to the conservation of the nanometric scale of the pore size distribution and the preservation of high specific surface area. The fine characterization of materials treated at 1900°C shows that a highly crystalline mesoporous SiC can be obtained, of a purely cubic polytype [22] compatible with a wide range of applications ranging from water filtration to electronics.

2. Materials and method

2.1. Chemicals

AHPCS of molecular mass between 1,500 and 3,000 g/mol was purchased from Starfire Systems, Inc. (reference SMP10 used below in the name of the samples), and SBS of polymer mass 140,000 g/mol was purchased from Sigma-Aldrich. These chemicals were used without further purification.

2.2. Analytical experiments

Infrared spectra were collected using a Perkin Elmer Spectrum 100 in Attenuated Total Reflectance (ATR) mode.

Nitrogen adsorption experiments were carried out on an ASAP 2020 at 77K. Samples were outgassed for 8 hours at 623 K until a 1 mmHg pressure was obtained prior to gas sorption measurements. The specific surface areas were determined using the BET method on 10 to 13 points of the adsorption isotherms, depending on the samples. The BET plots and fittings are available as supplementary information (Figure S1, S2 and S3). The porous distributions were estimated using the BJH model on the desorption branch of the isotherms.

Small and wide angle X-ray Scattering (SWAXS) was performed on a laboratory set up in transmission geometry, involving a Molybdenum anode delivering a wavelength of 0.71 Å after proper monochromatization by a Xenocs Fox3D multilayered mirror. A MAR345 2D imaging plate was used as detector and placed at about 750 mm from the sample position in order to record scattering intensity over a q-range between 0.2 and 30 nm^{-1}. X-ray diffraction (XRD) measurements were achieved with a Bruker D8 diffractometer in theta/theta geometry. The x-ray radiation from the Kα transition of a Cu anode (λ=1.54 Å) was used as incident excitation.

^{29}Si solid state nuclear magnetic resonance (NMR) was carried out on a Bruker Advance 400MHz

SEM/EDS observation were carried out on a FEI QUANTA 200 ESEM FEG, with an acceleration voltage of 30kV.

2.3. Materials preparation

In a typical experiment, 600 mg of SBS are introduced at ambient temperature in a flask under inert atmosphere with 25 mL of toluene and stirred until complete dissolution of SBS. The mixture is then heated at 70 °C and 40 µL of a 2 wt% solution of Karstedt catalyst in xylene are added. The color of the solution becomes light brown. A AHPCS solution made of 600 mg of AHPCS dissolved in 25mL of toluene is prepared under inert atmosphere in parallel. The AHPCS solution is then progressively introduced using an addition funnel, at a rate of one droplet every 3 s. After complete addition, the solution is maintained at 75°C under stirring for 24 h. Then, the SBS grafted with polycarbosilane (denoted [SBS-b-AHPCS]) can be recovered after solvent evaporation under reduced pressure (T=50 °C, P=50 mbar, 30 min). It alternatively may be further processed through cross-linking of the AHPCS by introducing in the medium $Cp_2Ti(OPh)_2$ (10 mg) beforehand dispersed in 5 mL of toluene (the preparation of the $Cp_2Ti(OPh)_2$ is described elsewhere [18]). Then, the mixture is kept at 75 °C for 48 h. The solvent can then be evaporated as described above and the grafted and cross-linked [SBS-b-AHPCS]r polycarbosilane is obtained. Finally, the polycarbosilane material is converted into porous SiC (denominated SBS-SMP) by pyrolysis in a tubular furnace under Ar atmosphere at 1000, 1300 or 1900°C for 2 hours after a 100°C/h increasing temperature ramp, and a free cooling down to ambient temperature.

Three synthesis conditions are summarized in Table 1.

Sample designation	SBS:SMP10 weight ratio	Synthesis condition
SBS-SMP-1	1:1	No $Cp_2Ti(OPh)_2$ cross linking
SBS-SMP-2	1:1	$Cp_2Ti(OPh)_2$ cross linking
SBS-SMP-3	2:1	$Cp_2Ti(OPh)_2$ cross linking

Table 1 : List and characteristics of the different samples studied. SMP-10 refers to the AHPCS.

Samples denoted SBS-SMP-1 and SBS-SMP-2 correspond to the final ceramic materials involving SBS / SMP-10 mixtures with a 1:1 weight ratio. Moreover, no titanocene-based catalyst is used in the case of SBS-SMP-1 sample to enhance the crosslinking after the recovery of the so-called [SBS-b-AHPCS] copolymer. On the contrary, the SBS-SMP-2 ceramic corresponds to the pyrolysis [SBS-b-AHPCS]r copolymer obtained after $Cp_2Ti(OPh)_2$ assisted cross linking. Finally the SBS-SMP-3 ceramic correspond to materials where the initial SBS /SMP—10 weight ratio was 2:1. Note that all ceramics have been pyrolyzed at 1000, 1300, or 1900°C.

3. Results and Discussion

Different characterizations were performed at each step of the process leading to the mesoporous SiC material. Emphasis is put on characterization techniques shedding new light on final materials with regards to those already published in [18]. The results are presented in the following according to the used characterization technique.

3.1. Infrared study

The SBS grafting on the SMP-10 preceramic polymer (involving Karstedt catalyst) has been already studied in our previous article [18]. Here we focus on the crosslinking step catalyzed by the titanocene-based catalyst, which we followed by infrared in ATR mode, for both sample SBS-SMP-2 before pyrolysis. The spectra of sample SBS-SMP-1, which was not submitted to the catalytic dehydrocondensation is shown for comparison in Figure 1a, as well as pure components spectra.

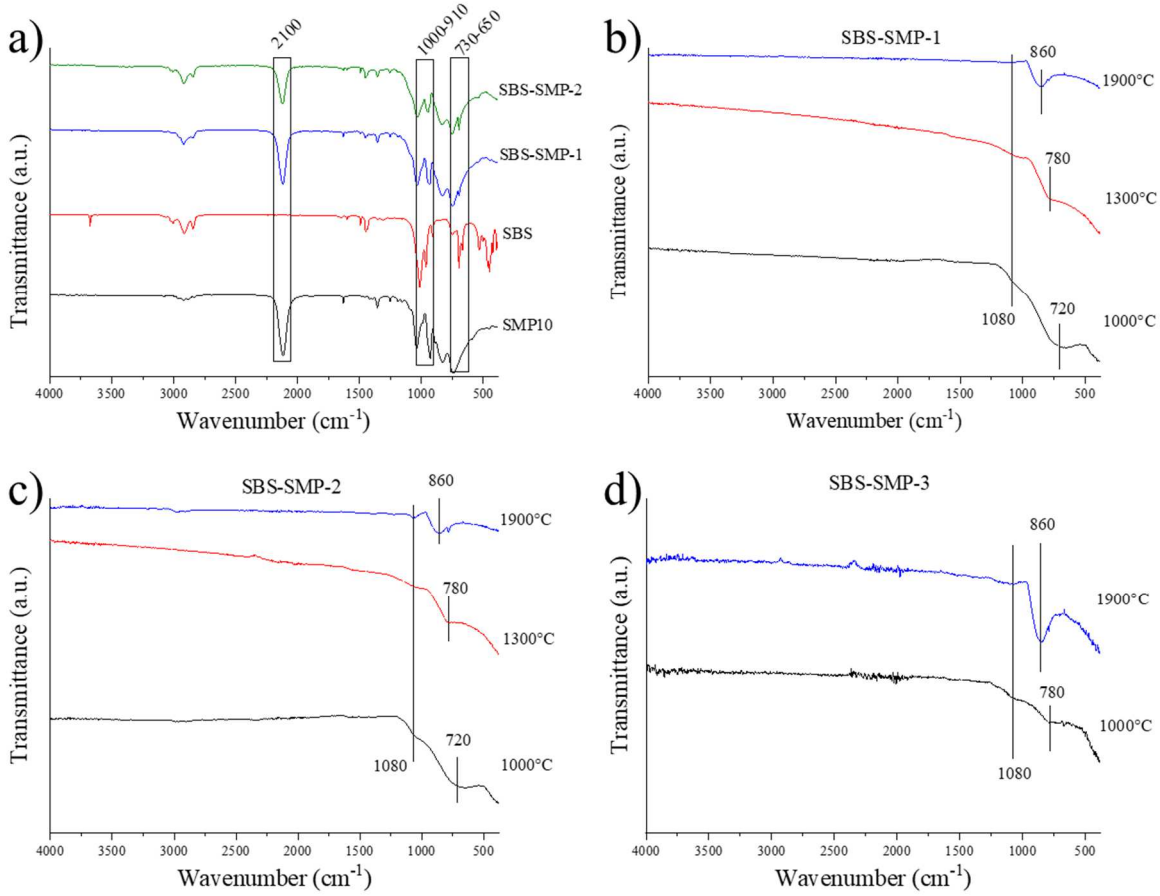

Figure 1 : Infrared spectra comparison of a) initial reagents (SBS and SMP10) and SBS-SMP-1 and 2 before pyrolysis, and pyrolyzed SiC from b) SBS-SMP-1, c) SBS-SMP-2, d) SBS-SMP-3 at different temperatures

The pure SBS spectrum shows polybutadiene double bond bands between 1000 and 910 cm^{-1} and between 730 and 650 cm^{-1} (Figure 1a). Unfortunately, SMP-10 also shows characteristic bands in the same spectral regions, preventing a fine analysis of the IR spectra of the mixtures. However, it seems that these bands are slightly less pronounced in the SBA-SMP-2

sample than in the SBS-SMP-1 samples. This would attest the consumption of the polybutadiene double bonds as the catalytic dehydrocondensation occurs [23]. The Si-H characteristic band at 2100 cm^{-1} of the SBS-SMP-2 sample also tends to decrease when compared to the pure SMP-10 spectrum, meaning the grafting of SMP-10 on SBS is effective [24] for this sample, in contrast to what is observed in the SBS-SMP-1 sample. This result confirms the conclusions drawn from Raman experiments on the same mixtures [18].

After pyrolyzed, grafted polymers are transformed into SiC. The IR spectra (Figure 1b, c and d) clearly show the modifications on the obtained materials. The Si-C absorption band is expected around 800 cm^{-1}, but its position strongly depends on the crystalline state of the SiC [25] . Then, after 1000°C pyrolysis, a large band between 780 and 720 cm^{-1} is visible for all samples, typical of amorphous SiC. After higher temperature treatment, the band progressively shifts to 860 cm^{-1} and becomes thinner, suggesting the crystallization of SiC. A weak band around 1080 cm^{-1} seems to appear on some of the spectra. It is known as a characteristic signal of silica Si-O bonds [24] . However, it is usually much more intense than the Si-C one. This means that in our samples, the surface pollution or oxidation of our materials remains low [26]. No signal is clearly distinguishable in the 3000 to 2800 cm^{-1} region for any sample, meaning that excess carbon is below the detection limit.

3.2. Nitrogen adsorption/desorption isotherms

Nitrogen adsorption/desorption isotherms have been investigated on the SiC materials in order to determine the specific surface area (SSA) and the pore size distribution of the materials according to the BET and BJH theory (except for SBS-SMP-3 1900°C, on which only a 10 points isotherm has been obtained in order to apply the BET method; a SSA of 70m^2/g was measured on this sample). Figure 2 summarizes these results.

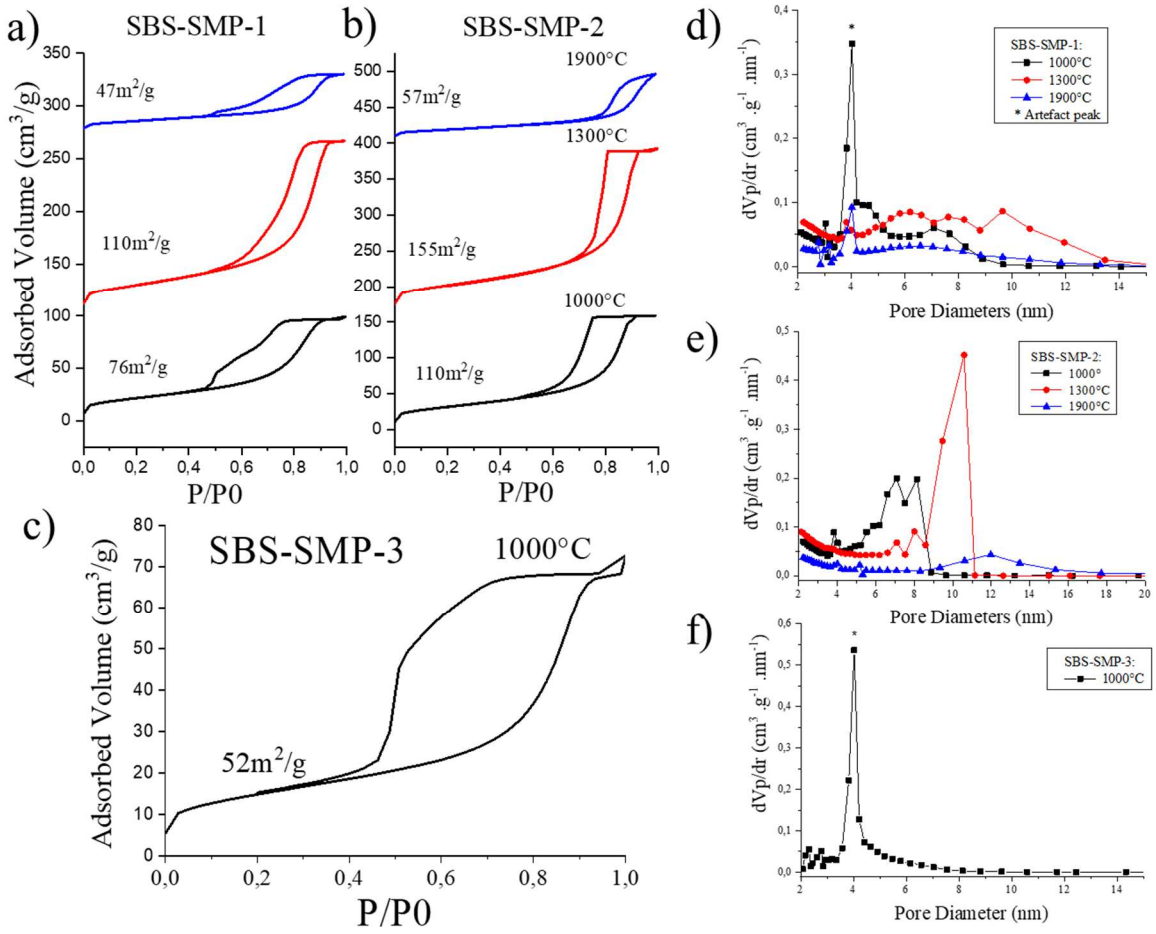

Figure 2 : Nitrogen adsorption/desorption isotherms of pyrolyzed a) SBS-SMP-1, b) SBS-SMP-2, and c) SBS-SMP-3 for different temperatures. Pore size distributions according to BJH calculation on desorption branch on pyrolyzed d) SBS-SMP-1, e) SBS-SMP-2 and f) SBS-SMP-3. Note that in a) the isotherms at 1300°C and 1900°C have been respectively shifted by 100 and 270 cm^3/g, and in b) by 160 and 400 cm^3/g for the sake of clarity. The sharp peak denoted * around 4nm in d) and f) comes from meniscus instability under desorption.

All isotherms present type IV profiles with H2 hysteresis according to the IUPAC classification [27] , showing the existence of mesoporosity with pores of disorganized sizes and shapes.

For SBS-SMP-1 and 2, which involve the same SBS:SMP ratio, an important SSA is measured from 1000 to 1300°C, which tends to increase with temperature. Such an increase of the SSA has already been discussed between 1000°C and 1500°C in SiC foams synthesized from boron-modified polycarbosilanes [28]. The authors attributed the SSA increase between 1000°C and 1300°C to the release of dihydrogen, creating microporosity in the sample due to the resulting empty spaces and the gas diffusion paths of leaving dihydrogen. This is in line with the increase of the contribution of pore sizes around 2 nm in the pore size distribution of the SBS-SMP-1 and SBS-SMP-2 heated at 1300°C with regards to that of the same samples heated at 1000°C (Figure 2d and 2e). Durif et al. also noted a further gas release involving oxygen-containing species above 1300°C and up to 1500°C, but as we did not consider

samples treated at the latter temperature, we can not comment on this observation. However, after a 1900°C pyrolysis, materials porosity strongly decreases. From the pore size distribution point of view (Figure 2d-f), the crosslinking step seems to result in a more homogeneous pore size distribution, as the SBS-SMP-2 sample shows a sharpened pore diameter distribution around 10 nm than SBS-SMP-1 after 1300°C pyrolysis. The overall pore diameter range remains similar for both samples (lower than 12 nm). This is in line with the shape of the isotherms, which display a hysteresis loop on similar pressure ranges, albeit with much more abrupt desorption branch for SBS-SMP-2. After pyrolysis at 1900°C, the porous volume collapses, explaining the decrease of the SSA. A more important fraction of microporosity could subsist in SBS-SMP-2 versus SBS-SMP-1, explaining the slightly higher value of SSA in the first sample. The pore distribution profile of SBS-SMP-3 at 1000°C is rather similar to that of SBS-SMP-1 at the same temperature, albeit the average pore value is slightly smaller. However, the parasite peak from meniscus instability at 4 nm prevents accurate analysis of the pore diameter distribution on these samples. Interestingly, the SBS-SMP-3 sample still shows a SSA of 70m²/g after a 1900°C pyrolysis treatment.

To summarize on the importance of the crosslinking step, we observe that SBS-SMP-2 systematically presents a SSA larger than that of SBS-SMP-1 by at least 20%. It also displays a sharpened pore diameter distribution, with a main contribution spreading over only 3 nm, while the main contribution of SBS-SMP-1 spreads over more than 10 nm for the same temperature treatment at 1300°C. Therefore, the crosslinking step appears to result in a better-organized structure of the final material, probably due to the increased cohesion of the precursor matrix that is less destabilized by the removal of the SBS templating polymer during the pyrolysis. Concerning the effect of the SBS:SMP-10 ratio, gas adsorption experiments were hard to exploit given the small mass of samples available. It appears that the increasing the mass fraction of templating agent (SBS) might increase the SSA of the sample at 1900°C.

It has been shown above by infrared spectroscopy that the SiC structure evolves as the pyrolysis temperature increases. According to the nitrogen adsorption/desorption study, these structural rearrangements also have an impact on the porosity, such as plugging or collapsing. The nature of the porous organization and evolution has been studied using SAXS and XRD.

3.3. Structure investigation by X-ray methods: SWAXS and XRD

SWAXS curves of SiC deriving from SBS-SMP-1, 2 and 3 after pyrolysis at different temperatures are shown in Figure 3.

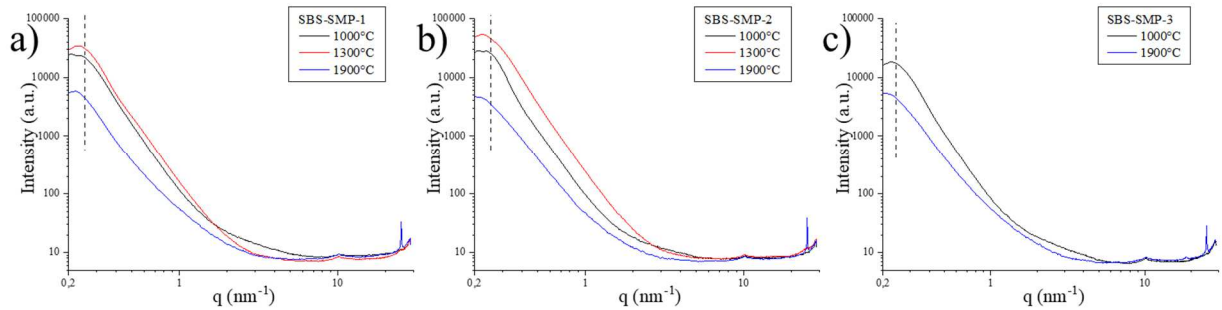

Figure 3 : SWAXS patterns of pyrolyzed SiC at different temperatures, a) SBS-SMP-1, b) SBS-SMP-2 and c) SBS-SMP-3.

Given the similar texture of our mesoporous granular samples, it is very difficult to compare the SWAXS profiles of the different samples [18]. However, valuable observations can be made by following the SWAXS profile of one sample with its pyrolysis temperature. At the lowest scattering vectors reachable with our experimental set up, an intense peak can be resolved (left side of dashed bars in Figure 3), testifying to a characteristic distance in the [20-30 nm] range in the probed samples. Such a distance is in line with a typical pore center to pore center distance. Moreover, for each initial preparation, the higher temperature pyrolysis seems to result in a shift of the maximum position to the lower scattering vectors. This means that the characteristic distance is further increased with the increase of pyrolysis temperature. This is quite surprising as the SiC densification could rather result in a contraction of the distances in the sample. Considering the SWAXS patterns of the samples pyrolyzed at 1900°C in the Porod region (0,25 – 1 nm^{-1}), it also appears that the intensity is always lower than for the other temperatures. This can be related to a decrease of the SSA at 1900°C, in good agreement with the BET results discussed above. Moreover, the slope of intensity vs scattering vector appears smaller in the 1900°C-treated samples, meaning that the wall/pore interface in these samples has become less sharp. All these observations could be related to a pore coalescence phenomenon [29].

SWAXS patterns also show the emergence of a Bragg peak at 25 nm^{-1} after pyrolysis at 1900°C. This peak illustrates the SiC transformation from amorphous to crystalline β-SiC. The latter peak in SAXS data corresponds to the first peak observed on the XRD patterns reported in Figure 4.

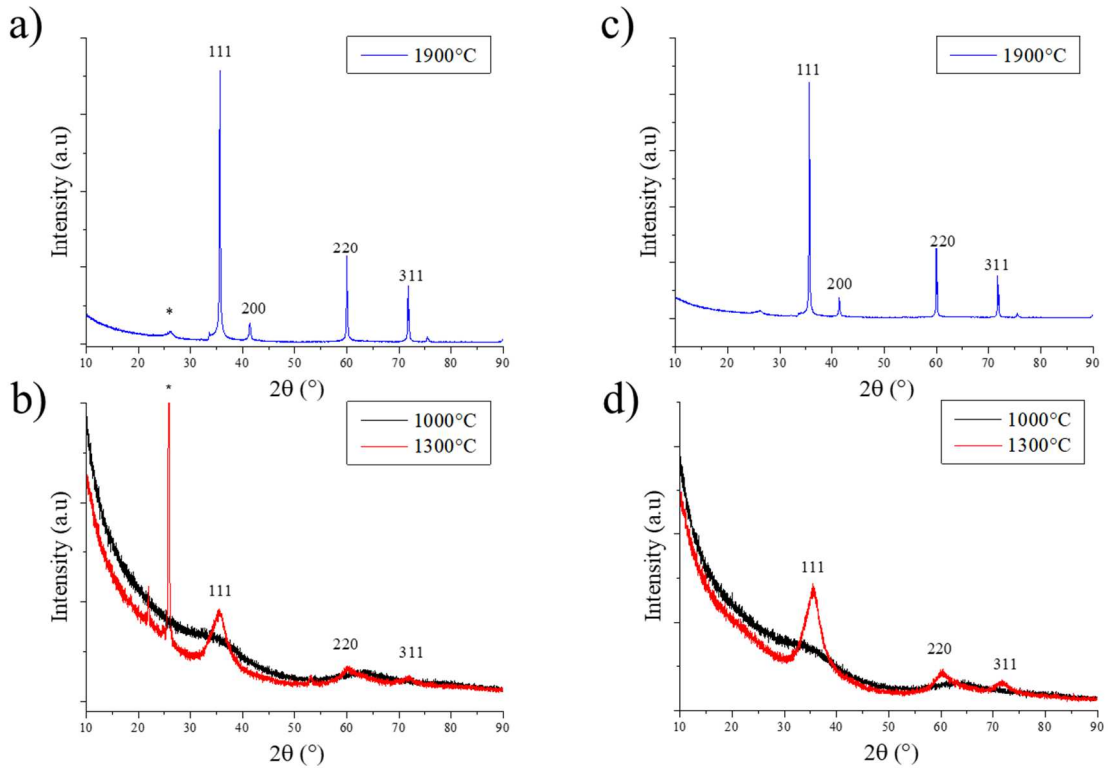

Figure 4 : XRD diagrams of pyrolyzed SiC originating from a) SBS-SMP-1 at 1900°C (a), 1000°C and 1300°C (b), and SBS-SMP-2 at 1900°C (c), 1000°C and 1300°C (d). The star in (a) and (b) is attributed to the 002 peak of graphite.

From 1000 to 1900°C, XRD clearly shows the progressive crystallization process of SiC with the emergence of four peaks. At 1000°C, only badly defined bumps are visible, and SiC is mainly under amorphous form. At 1300°C, the 111, 220 and 311 peaks of the cubic β-SiC structure rise from the bumps, showing a partial crystallization of the SiC. After 1900°C treatment, the SiC cubic face centered structure is well-defined by diffraction peaks [21,30]. It therefore appears here that we were able to produce a highly crystalline β-SiC of large SSA, for which the bandgap of 2.3 eV [31] opens interesting applications for the photodegradation of organic pollutants in water. The peak marked with * around 2θ=26° in the SBS-SMP-1 sample heated at 1300°C does not belong to the SiC structure. According to other references, it is likely to originate from graphitic carbon (002 peak of graphite). It could come from the carbon excess in Si:C ratio induced by SBS [32,33]. The intensity of the 002 peak of graphite is known to be considered with precaution for quantification as it can strongly vary depending on the orientation of graphite crystallites with regards to the x-ray beam. Its absence in SBS-SMP-2 derived XRD patterns at 1000 and 1300°C, and its very weak intensity in XRD patterns at 1900°C underlines the fact that graphite is present in very small quantities. Given these XRD results, together with SEM and EDS results discussed below, graphite is likely to be located in the outer surface of some of the grains, and represents a small fraction of the sample.

At this stage, we have demonstrated the elaboration of highly crystalline β-SiC showing high SSA and pore sizes below 10 nm. ^{13}C and ^{29}Si solide-state NMR on our SiC materials allowed us to get more insight on the SiC structure and its oxidation state.

3.4. Solid ^{13}C and ^{29}Si NMR

Solid ^{13}C and ^{29}Si NMR studies have been carried out on the SBS-SMP-2 sample after 1000 and 1900°C pyrolysis. The results are presented on Figure 5. The study was restricted to this sample due to the time consuming character of these experiments. Therefore, the conclusions drawn from these experiments only concern SiC materials derived from SBS-SMP-2 preparation.

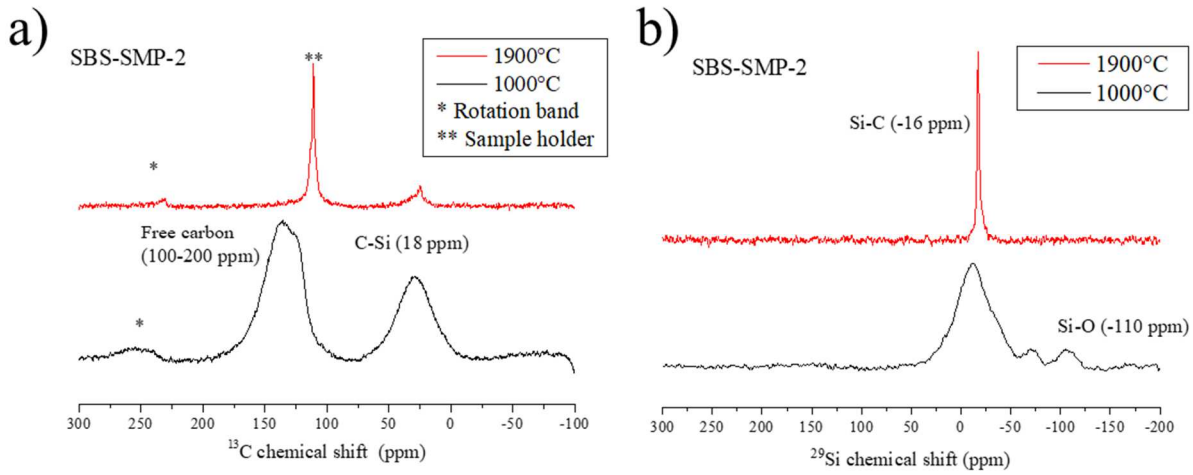

Figure 5 : a) ^{13}C and b) ^{29}Si NMR spectra of SBS-SMP-2 pyrolyzed at 1000 and 1900°C

After a 1000°C pyrolysis, the ^{13}C NMR spectrum (lower curve in Figure 5a) shows two signals, at 130 and 30ppm, respectively attributed to free carbon and amorphous SiC [21,34]. The ^{29}Si spectrum of the same sample (lower curve in Figure 5b) confirms the presence of amorphous SiC with a -10 ppm shift, but the bumps at -70 and -110 ppm also indicate the presence of SiO_4 species [32,35], albeit at significantly lower intensity level. As NMR intensities reflect actual composition, the latter silica signal can be attributed to non-significant pollution, which do not appear on XRD patterns.

At 1900°C, the free carbon signal in ^{13}C NMR spectrum (upper curve in Figure 5a) is masked under the signal coming from the sample holder (** in Figure 5a), but a thinner crystallized SiC peak is clearly visible on both ^{13}C and ^{29}Si spectra [34]. It is worthy to note that Si-O bands disappeared, as at such a high temperature, any trace of silica is expected to be degraded.

3.5. Scanning Electronic Microscopy and EDS

All the previously presented SiC samples, i.e. SBS-SMP-1, 2 and 3 pyrolyzed at 1000, 1300 and 1900°C, have been observed by SEM in order to get more information on the textural morphology of these samples. These observations allow us to morphologically and chemically differentiate two zones in these SiC materials.

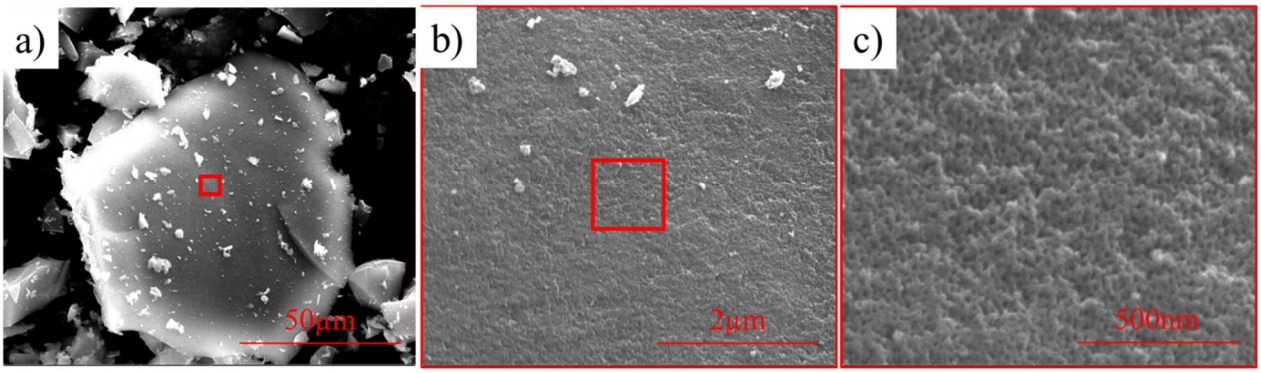

Figure 6 : SEM pictures of SBS-SMP-1 grain pyrolyzed at 1000°C in progressive magnification from a) to c) represented by red square.

Figure 6 shows a progressive magnification on a SiC sample from SBS-SMP-1 pyrolyzed at 1000°C. Direct measurements using the Fiji software [36] reveal pores diameters values from 6 to 14 nm and pore center to pore center distances ranging between 20 and 40 nm. Same treatment on SBS-SMP-2 (Figure 7a) leads to pore diameters between 8 and 11 nm, and 25 to 40 nm for pore center to pore center distances. These measures are in good agreement with both BJH calculation and SAXS features at the lower scattering vector values. Moreover, the TEM image shown on Figure 7b confirms the presence of a not organized mesoporosity and allows estimating the wall thickness, which is of a dozen of nanometers, reinforcing previous BJH and SAXS results.

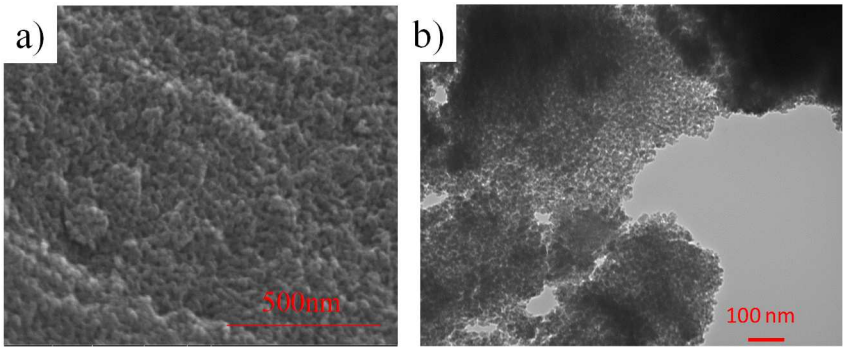

Figure 7 : SEM a) and TEM b) pictures of SBS-SMP-2 pyrolyzed at 1000°C.

Lower magnifications displayed in Figure 8 show different surface morphologies, and in particular that porosity can be trapped behind a crust. Despite the porous area, whose texture could be described as “sponge-like”, another area appears more wrinkled. Observation of such areas has been made on SBS-SMP-2 and 3 pyrolyzed at 1000°C.

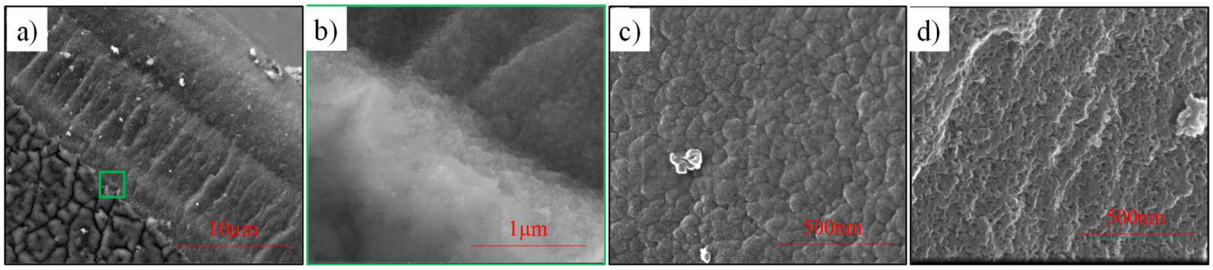

Figure 8 : SEM images of a) SBS-SMP-2 pyrolyzed at 1000°c showing both the crust and the sponge-like area, b) magnification of the area highlighted by the green square in a), c) a crust area and d) a sponge-like area in a SBS-SMP-3 pyrolyzed at 1000°C.

On Figure 8a and b, the magnification has been centered on the intermediate point between the wrinkled and sponge like morphologies. It appears that the wrinkled area could be assimilated to a crust around SiC grains, with no visible porosity, around porous SiC appearing as the sponge-like part. The typical width of such crusts, when observed, is of about 10 µm, around grains larger than 100 µm. The coexistence of these two surface morphologies is confirmed in the SiC sample resulting from the SBS-SMP-3 pyrolysis at 1000°C, as depicted on Figure 8c and d. The pore size was measured between 9 and 11 nm (in good agreement with BJH calculations), and center-to-center pore distances between 25 and 40 nm (in good agreement with SAXS observations). We resume the main structural parameters we measured on the different samples in Table 2, which displays the SSA, mesopore diameter distribution, and inter-pore mean distance of the samples at different temperatures.

Sample designation	Pyrolysis temperature	SSA (m^2/g)	Mesopore diameter distribution (nm; BJH/SEM)	Mean inter-pore distance (nm;SEM)
SBS-SMP-1	1000°C	76	4–8 / 6–14	20 – 40
	1300°C	110	4–12	20 – 40
	1900°C	47	3–12	*High heterogeneity*
SBS-SMP-2	1000°C	110	6–8 / 8–11	25 – 40
	1300°C	155	9–11	25 – 40
	1900°C	57	10–14	*High heterogeneity*
SBS-SMP-3	1000°C	52	3-6 / 9–11	25 – 40
	1300°C	n.a.	n.a.	25 – 40
	1900°C	70	n.a.	*High heterogeneity*

Table 2: Main structural parameters of the SiC samples pyrolyzed at 1000°C, 1300°C and 1900°C from gas adsorption and SEM measurements.

SBS-SMP-1 and 2 samples pyrolyzed at 1300°C present the same morphologies than samples pyrolyzed at 1000°C. Examples are given on Figure 9. It is noteworthy that the inner sponge-like morphology related to the porous area is visible through cracks on these samples. Considering a large number of SEM images, SBS-SMP-1 pyrolyzed at 1300°C seems quantitatively less organized than its “crosslinked” equivalent from SBS-SMP-2. The

crosslinking step is likely to allow the initial reticulated matrix to keep a stronger cohesion while template destruction. This stronger cohesion results in a better-organized structure, which is maintained during the amorphous SiC crystallization into β-SiC.

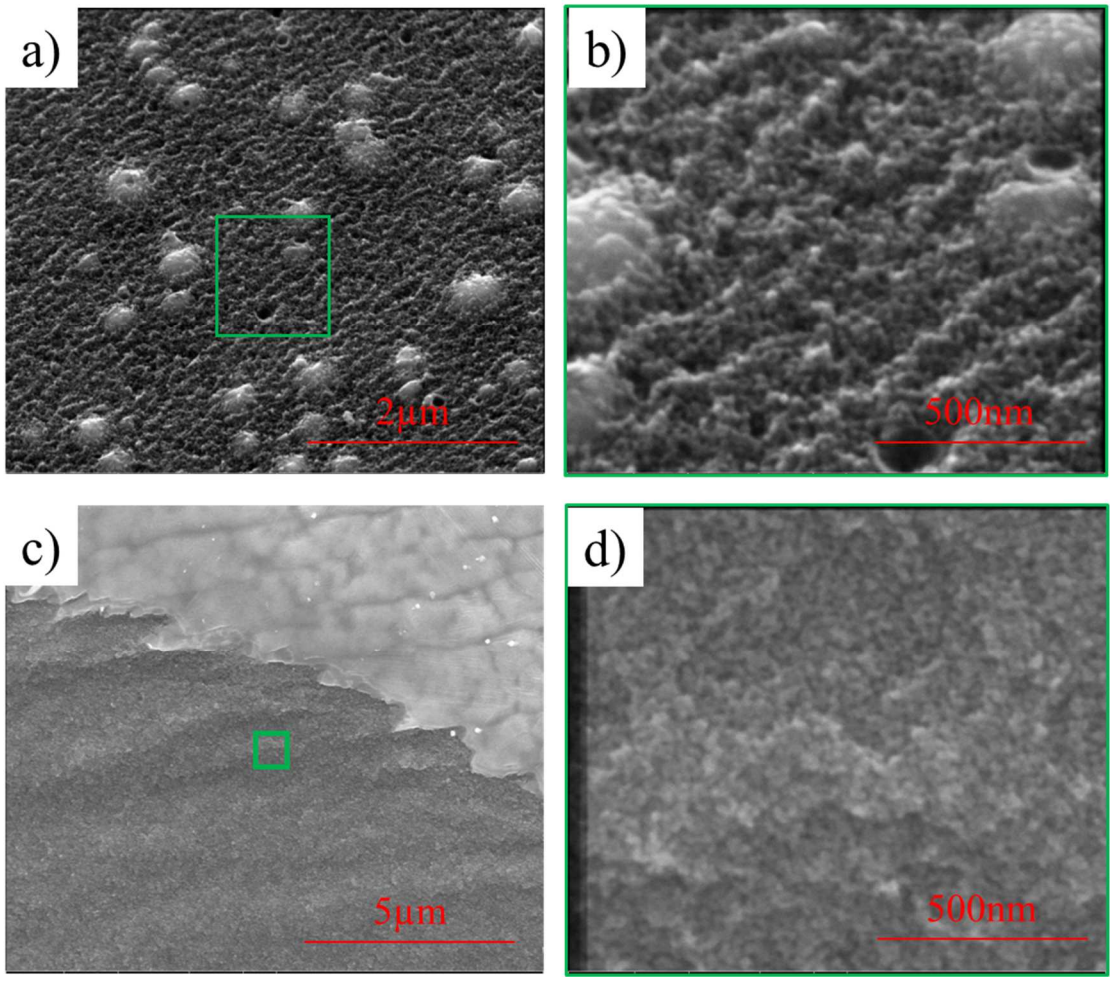

Figure 9 : SEM images of SBS-SMP-1 (a, b) and SBS-SMP-2 (c, d) pyrolyzed at 1300°C.

Finally, samples pyrolyzed at 1900°C (Figure 10) show drastic changes in their morphology, as expected regarding pore size distributions derived from BJH calculations. The sponge-like areas appear in a lesser extent, while other regions with sharper edges show up. This could be induced by SiC crystallization, and is in line with the SSA decrease by pores deformation and clogging.

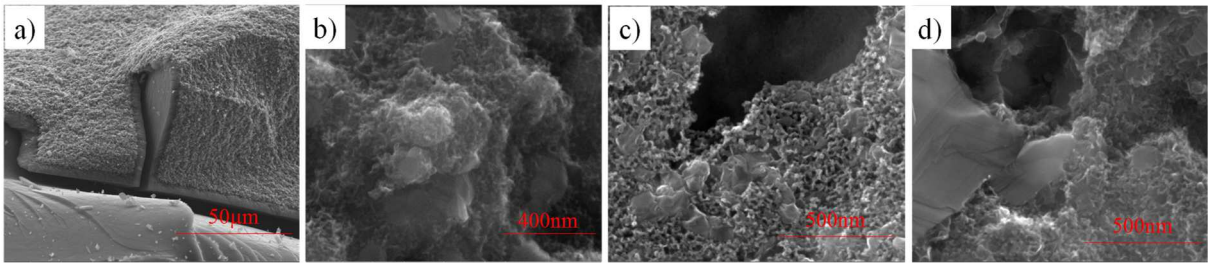

Figure 10 : SEM images of SiC samples after pyrolysis at 1900°C: a) SBS-SMP-1 derived crust and porous area large view, and magnification on porosity of b) SBS-SMP-1, c) SBS-SMP-2 and d) SBS-SMP-3 derived samples.

In order to get a better understanding of the chemical nature of the crust and sponge-like parts of the SiC materials, EDS analyses were performed on all samples obtained after pyrolysis at 1900°C. Results are summarized on Figure 11.

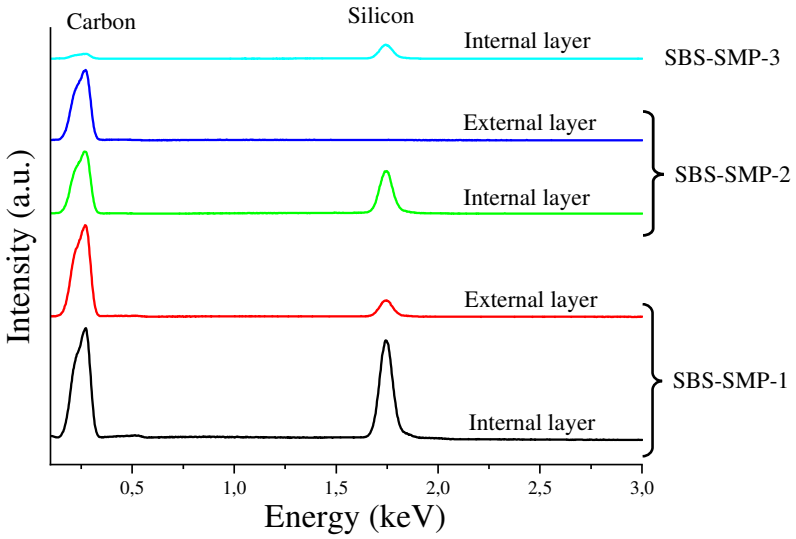

Figure 11 : EDS spectra of SiC from aSBS-SMP-1, SBS-SMP-2, and SBS-SMP-3 pyrolyzed at 1900°C, recorded on both the crust (outer shell) and sponge-like (inner shell) areas.

Based on these results and on previous SEM observations, the wrinkled crust appears to be mainly composed of carbon. On the contrary, silicon and carbon appear with a similar ratio in the inner sponge-like part, confirming the SiC nature of the latter part. The excess carbon introduced by the SBS template could be at the origin of the crust. In order to get rid of this crust that possibly restricts the SSA due to the associated pore closure, a thermal treatment under air could be considered. It is worth noting that for all areas measured, the oxygen signal (expected at ~ 0.5 keV) is barely measureable, proving that no oxygen remains in the samples after pyrolysis at 1900°C.

4. Conclusion

SiC presenting high SSA were obtained using a soft-templating approach involving SBS as polymeric templates. Different protocols were considered. They allowed us to measure the effect i) of a crosslinking step of the polycarbosilane precursor after grafting on SBS, ii) of the variation of the SBS:polycarbosilane ration in the starting mixture, and iii) of the pyrolysis temperature on all the original mixtures. The crosslinking step using $Cp_2Ti(OPh)_2$ proved it efficiency in providing SiC materials showing larger SSA, whatever the pyrolysis temperature. This step appears to render the material more resilient during the templating agent removal, and therefore results in a better defined porous structure in the final material, i.e. after pyrolysis is complete. It was shown that the higher the pyrolysis temperature, the higher the crystallization state of the SiC. The highest pyrolysis temperature (1900°C) is believed to promote atomic rearrangements in the material structure, leading to pore

collapsing and/or clogging. However, the remaining porosity on well-crystallized SiC is far from negligible. It has to be noted that SSA larger than 50 m^2/g are obtained in SiC materials with very high crystallinity and presenting a pore diameter lower than 10 nm. These characteristics are very unusual and could be highly valuable for nanofiltration applications. Modification of the 1:1 SBS:SMP10 ratio led to a lowering of the SSA after a 1000°C temperature treatment, but the SSA was conserved and even slightly increased at higher temperature. SiC samples were proven to contain a small amount of carbon, located at the grain edges, probably originating from SBS template. The carbon content is very hard to quantify, but it is likely to be low (i.e. less than 5 at.%) given XRD and EDS analyses. SiC samples appear preserved from oxidation. New temperature treatments under airflow could be envisioned to remove excess carbon, as once SiC became inert, its oxidation into silica becomes unlikely.

Acknowledgments

The authors acknowledge the ANR for funding the FANTA-SiC project (ANR-12-JS08-0010) and the CNRS for funding the NoStra-SiC project. Henri-Pierre Brau and Renaud Podor are thanked for assistance in SEM experiments as well as Bruno Corso in SWAXS experiments, and Clémentine Mansas in TEM experiments. Jeremy Causse is thanked for assistance in gas sorption experiments.

References

[1] W. Wei, W. Zhang, Q. Jiang, P. Xu, Z. Zhong, F. Zhang, W. Xing, Preparation of non-oxide SiC membrane for gas purification by spray coating, J. Memb. Sci. 540 (2017) 381–390. https://doi.org/10.1016/j.memsci.2017.06.076.

[2] Y. Zhang, Y. Hu, H. Zeng, L. Zhong, K. Liu, H. Cao, W. Li, H. Yan, Silicon carbide recovered from photovoltaic industry waste as photocatalysts for hydrogen production, J. Hazard. Mater. 329 (2017) 22–29. https://doi.org/10.1016/j.jhazmat.2017.01.023.

[3] X. Han, D. Wang, Z. Guo, L. Huang, Y. Peng, J. Lin, W. Yuan, Excellent visible light absorption by adopting mesoporous SiC in SiC/CdS for enhanced photocatalytic hydrogen generation, Mater. Express. 9 (2019) 65–72. https://doi.org/10.1166/mex.2019.1469.

[4] M.C. Bruzzoniti, M. Appendini, L. Rivoira, B. Onida, M. Del Bubba, P. Jana, G.D. Sorarù, Polymer-derived ceramic aerogels as sorbent materials for the removal of organic dyes from aqueous solutions, J. Am. Ceram. Soc. 101 (2018) 821–830. https://doi.org/10.1111/jace.15241.

[5] R. Masson, V. Keller, N. Keller, β-SiC alveolar foams as a structured photocatalytic support for the gas phase photocatalytic degradation of methylethylketone, Appl. Catal. B Environ. 170–171 (2015) 301–311. https://doi.org/10.1016/j.apcatb.2015.01.030.

[6] V. Médout-Marère, A. El Ghzaoui, C. Charnay, J.M. Douillard, G. Chauveteau, S. Partyka, Surface heterogeneity of passively oxidized silicon carbide particles: Hydrophobic-hydrophilic partition, J. Colloid Interface Sci. 223 (2000) 205–214. https://doi.org/10.1006/jcis.1999.6625.

[7] Y. Kim, K. Min, J. Shim, D.J. Kim, Formation of porous SiC ceramics via recrystallization, J. Eur. Ceram. Soc. 32 (2012) 3611–3615. https://doi.org/10.1016/j.jeurceramsoc.2012.04.044.

[8] P. Krawiec, C. Weidenthaler, S. Kaskel, D. Mu, SiC / MCM-48 and SiC / SBA-15 Nanocomposite Materials, (2004) 2869–2880.

[9] T. Nardin, J. Cambedouzou, J. Ravaux, C. Rey, D. Meyer, O. Diat, Elaborating ordered silicon carbide nanorods by preceramic polymer nanocasting, RSC Adv. 5 (2015) 86156–86162. https://doi.org/10.1039/c5ra17376k.

[10] Y. Zhong, R. Kou, M. Wang, Y. Qiao, Synthesis of centimeter-scale monolithic SiC nanofoams and pore size effect on mechanical properties, J. Eur. Ceram. Soc. 39 (2019) 2566–2573. https://doi.org/10.1016/j.jeurceramsoc.2019.02.023.

[11] T. Nardin, B. Gouze, J. Cambedouzou, P. Bauduin, M. Wong Chi Man, X. Deschanels, D. Bourgeois, D. Meyer, O. Diat, Elaboration of porous silicon carbide by soft templating molecular precursors with semi-fluorinated alkanes, J. Mater. Chem. A. 3 (2015) 3082–3090. https://doi.org/10.1039/c4ta05996d.

[12] B. Gouze, T. Nardin, O. Diat, J. Cambedouzou, Aggregation of semifluorinated alkanes in cyclic organic solvents: A SAXS study, Colloids Interface Sci. Commun. 31 (2019) 100189. https://doi.org/10.1016/j.colcom.2019.100189.

[13] L. Borchardt, M. Oschatz, M. Lohe, V. Presser, Y. Gogotsi, S. Kaskel, Ordered mesoporous carbide-derived carbons prepared by soft templating, Carbon N. Y. 50 (2012) 3987–3994. https://doi.org/10.1016/j.carbon.2012.04.006.

[14] R. Sreeja, B. Swaminathan, A. Painuly, T. V. Sebastian, S. Packirisamy, Allylhydridopolycarbosilane (AHPCS) as matrix resin for C/SiC ceramic matrix composites, Mater. Sci. Eng. B Solid-State Mater. Adv. Technol. 168 (2010) 204–207. https://doi.org/10.1016/j.mseb.2009.12.033.

[15] Q.D. Nghiem, D.P. Kim, Direct preparation of high surface area mesoporous SiC-based ceramic by pyrolysis of a self-assembled polycarbosilane-block-polystyrene diblock copolymer, Chem. Mater. 20 (2008) 3735–3739. https://doi.org/10.1021/cm702688j.

[16] Y. Yu, X. Yang, C. Xu, J. Fang, L. An, Synthesis of nanostructured silicon carbide at ultralow temperature using self-assembled polymer micelles as a precursor, J. Mater. Chem. 21 (2011) 17619–17622. https://doi.org/10.1039/c1jm13973h.

[17] X. Yang, Y. Chen, J. Fang, L. An, Formation of hierarchical mesoporous silicon carbide from self-assembled block copolymer micelles, Mater. Lett. 190 (2017) 195–197. https://doi.org/10.1016/j.matlet.2016.12.029.

[18] T. Nardin, B. Gouze, J. Cambedouzou, O. Diat, Soft templated mesoporous SiC from polycarbosilane grafted onto triblock copolymers, Mater. Lett. 185 (2016) 424–427. https://doi.org/10.1016/j.matlet.2016.09.041.

[19] T.P. Lodge, Block copolymers: Past successes and future challenges, Macromol. Chem. Phys. 204 (2003) 265–273. https://doi.org/10.1002/macp.200290073.

[20] L.M. Rueschhoff, L.A. Baldwin, R. Wheeler, M.J. Dalton, H. Koerner, J.D. Berrigan,

N.M. Bedford, S. Seifert, M.K. Cinibulk, M.B. Dickerson, Fabricating Ceramic Nanostructures with Ductile-like Compression Behavior via Rapid Self-Assembly of Block Copolymer and Preceramic Polymer Blends, ACS Appl. Nano Mater. 2 (2019) 250–257. https://doi.org/10.1021/acsanm.8b01820.

[21] R.M. Laine, F. Babonneau, Preceramic Polymer Routes to Silicon Carbide, Chem. Mater. 5 (1993) 260–279. https://doi.org/10.1021/cm00027a007.

[22] F. Delobel, S. Lemonnier, É. Barraud, J. Cambedouzou, Influence of sintering temperature and pressure on the 3C-6H transition of silicon carbide, J. Eur. Ceram. Soc. 39 (2019) 150–156. https://doi.org/10.1016/j.jeurceramsoc.2018.09.010.

[23] J.L. Binder, The Infrared Spectra and Structures of Polybutadienes, J. Polym. Sci. A 1 (1963) 47–58. doi:10.1002/pol.1963.100010105.

[24] P.J. Launer, Infrared analysis of organosilicon compounds: spectra-structure correlations, Silicone Compd. Regist. Rev. (1987) 100–103.

[25] M. Dkaki, L. Calcagno, A.M. Makthari, V. Raineri, Infrared spectroscopy and transmission electron microscopy of polycrystalline silicon carbide, Mater. Sci. Semicond. Process. 4 (2001) 201–204. https://doi.org/10.1016/S1369-8001(00)00113-X.

[26] J. Wang, M. Oschatz, T. Biemelt, M.R. Lohe, L. Borchardt, S. Kaskel, Preparation of cubic ordered mesoporous silicon carbide monoliths by pressure assisted preceramic polymer nanocasting, Microporous Mesoporous Mater. 168 (2013) 142–147. https://doi.org/10.1016/j.micromeso.2012.09.037.

[27] S. Lowell, J.E. Shields, M.A. Thomas, M. Thommes, Characterization of Porous Solids and Powders: Surface Area, Pore Size and Density, Springer Netherlands, Dordrecht, 2004. https://doi.org/10.1007/978-1-4020-2303-3.

[28] C. Durif, M. Wynn, M. Balestrat, G. Franchin, Y.-W. Kim, A. Leriche, P. Miele, P. Colombo, S. Bernard, Open-celled silicon carbide foams with high porosity from boron-modified polycarbosilanes, J. Eur. Ceram. Soc. 39 (2019) 5114–5122. https://doi.org/10.1016/j.jeurceramsoc.2019.08.012.

[29] O. Spalla, S. Lyonnard, F. Testard, Analysis of the small-angle intensity scattered by a porous and granular medium, J. Appl. Crystallogr. 36 (2003) 338–347. https://doi.org/10.1107/S0021889803002279.

[30] G.Q. Jin, X.Y. Guo, Synthesis and characterization of mesoporous silicon carbide, Microporous Mesoporous Mater. 60 (2003) 207–212. https://doi.org/10.1016/S1387-1811(03)00378-0.

[31] C. Persson, U. Lindefelt, Relativistic band structure calculation of cubic and hexagonal SiC polytypes. J. Appl. Phys. 82, 11 (1997) 5496-5508. https://doi.org/10.1063/1.365578.

[32] G.D. Soraru, F. Babonneau, J.D. Mackenzie, Structural evolutions from polycarbosilane to SiC ceramic, J. Mater. Sci. 25 (1990) 3886–3893. https://doi.org/10.1007/BF00582455.

[33] Y. Hasegawa, Synthesis of continuous silicon carbide fibre: Part 6 Pyrolysis process of

cured polycarbosilane fibre and structure of SiC fibre, J. Mater. Sci. 24 (1989) 1177–1190. https://doi.org/10.1007/BF02397045.

[34] I.K. Sung, Christian, M. Mitchell, D.P. Kim, P.J.A. Kenis, Tailored macroporous SiCN and SiC structures for high-temperature fuel reforming, Adv. Funct. Mater. 15 (2005) 1336–1342. https://doi.org/10.1002/adfm.200500038.

[35] B. Gouze, J. Cambedouzou, S. Parrès-Maynadié, D. Rébiscoul, How hexagonal mesoporous silica evolves in water on short and long term: Role of pore size and silica wall porosity, Microporous Mesoporous Mater. 183 (2014) 168–176. https://doi.org/10.1016/j.micromeso.2013.08.041.

[36] J. Schindelin, I. Arganda-Carreras, E. Frise, V. Kaynig, M. Longair, T. Pietzsch, S. Preibisch, C. Rueden, S. Saalfeld, B. Schmid, J.Y. Tinevez, D.J. White, V. Hartenstein, K. Eliceiri, P. Tomancak, A. Cardona, Fiji: An open-source platform for biological-image analysis, Nat. Methods. 9 (2012) 676–682. https://doi.org/10.1038/nmeth.2019.